Unclassified
Report No. NADC-78240-60

LASER GENERATED ELASTIC WAVES FOR ULTRASONIC EVALUATION

R. J. von Gutfeld
IBM Thomas J. Watson Research Center
Yorktown Heights, New York 10598

Final Report for Work Performed
June 79 - June 80

Approved for Public Release
distribution unlimited

Prepared for
Naval Air Development Center
Department of the Navy
Warminster, PA 18974

Unclassified

International Business Machines Corporation

Thomas J. Watson Research Center
P.O. Box 218
Yorktown Heights, New York 10598
914/945-3000

September 10, 1980

Dr. William Scott NADC 6063
Naval Air Development Center
Warminster, Pennsylvania 18974

Dear Sir:

Subject: Contract N62269-79-C-0208

In accordance with Item A003 of the subject contract Data Requirements List (DD Form 1423) enclosed are forty copies of the Final Technical Report.

Very truly yours,

E. K. Woelfle

Eileen K. Woelfle
Administrative Analyst

cc: NADC 813 (w/encl. 2) ✓
ACO, DCASMA, N.Y.

Unclassified

SECURITY CLASSIFICATION OF THIS PAGE (When Data Entered)

REPORT DOCUMENTATION PAGE		READ INSTRUCTIONS BEFORE COMPLETING FORM
1. REPORT NUMBER NADC-78240-60	2. GOVT ACCESSION NO.	3. RECIPIENT'S CATALOG NUMBER
4. TITLE (and Subtitle) Laser Generated Elastic Waves for Ultrasonic Evaluation		5. TYPE OF REPORT & PERIOD COVERED Final Report 6/79-6/80 6. PERFORMING ORG. REPORT NUMBER
7. AUTHOR(s) R. J. von Gutfeld		8. CONTRACT OR GRANT NUMBER(s) N62269-79-C-0208
9. PERFORMING ORGANIZATION NAME AND ADDRESS IBM Thomas J. Watson Research Center P.O. Box 218 Yorktown Heights, New York 10598		10. PROGRAM ELEMENT, PROJECT, TASK AREA & WORK UNIT NUMBERS
11. CONTROLLING OFFICE NAME AND ADDRESS Naval Air Development Center Warminster, Pa. 18974		12. REPORT DATE June 25, 1980 13. NUMBER OF PAGES 48
14. MONITORING AGENCY NAME & ADDRESS(if different from Controlling Office)		15. SECURITY CLASS. (of this report) Unclassified 15a. DECLASSIFICATION/DOWNGRADING SCHEDULE

16. DISTRIBUTION STATEMENT (of this Report)

Approved for public release; distribution unlimited.

17. DISTRIBUTION STATEMENT (of the abstract entered in Block 20, if different from Report)

18. SUPPLEMENTARY NOTES

19. KEY WORDS (Continue on reverse side if necessary and identify by block number)

20. ABSTRACT (Continue on reverse side if necessary and identify by block number)

A summary of work using lasers to generate elastic waves for NDT is presented. Included is work on flaw detection of small holes, simulated cracks and varying film thicknesses of several samples. Calculations on thermal profiles for a number of multi-layered configurations is presented. Experiments on beam profiling and photoacoustics in relation to flaw detection are described.

DD FORM 1 JAN 73 1473 EDITION OF 1 NOV 65 IS OBSOLETE

Unclassified

SECURITY CLASSIFICATION OF THIS PAGE (When Data Entered)

TABLE OF CONTENTS

LIST OF FIGURES

LIST OF TABLES

I. FLAW DETECTION

INTRODUCTION

We investigated several variations of previously described techniques in which elastic waves generated by laser induced thermoelastic expansions are used for flaw detection.[1,2] In particular we have attempted to take advantage of the enhancement of the elastic amplitude that occurs by mechanical clamping of the laser absorbing surface. In the present experiments we again used 5 nsec laser pulses from a pulsed nitrogen dye laser to serve as the excitation source but in place of the dielectric clamp we have used water as the constraining medium.[3] At 10 MHz water is only a factor of 2 less effective than a dielectric rigid clamp such as fused quartz plate.[1] The use of water as mechanical constraint has several advantages 1) the assurance of uniform acoustic contact between the clamping medium and the sample under test, virtually irrespective of surface curvature and 2) provision for uniform coupling between sample and piezoelectric detector when an immersion receiver is used as the detector.

EXPERIMENT AND RESULTS

1. Bulk Samples

The experimental arrangement is shown in Figure 1. The dye laser was operated at low repetition rates, typically 15 Hz with incident power on the order of 40–150 Watts. The output of the PZT immersion detector (10 MHz, 6 mm diameter, Aerotech) was amplified 40 dB prior to the box integrator and chart recorder output. A water tank was designed for studying flaws in samples on the order of 1 cm or less on a side with the entire tank sufficiently small to fit onto the stage of a microscope. The objective lens served to focus the laser light to spot diameters on the order of $5\times10^{1}-10^{3}\mu$. Specimens of Al, Ti and graphite-epoxy were investigated (laminated graphite-epoxy samples supplied by NADC). In the metal samples, we attempted to obtain signals in transmission with scattering occurring from mechanically drilled edge and through holes varying between 0.036 to 0.1 cm in diameter. Scanning of the cylindrical flaws was achieved by micrometer movement of the sample assuring constant alignment between the incident laser and PZT detector. This method of

thermoelastic excitation requires that the optical absorption of the sample be uniform over the surface so that the amplitudes of the generated waves are equal for all points of interrogation. In order to avoid this requirement which is rarely realized unless special polishing of the surface is undertaken, an alternate method was devised in which a thin rubber membrane was interposed between the laser and the sample. The membrane with its large absorption constant and large thermal expansion coefficient serves as the thermoelastic generator, fixed in position. The configuration is shown in Figure 2.

Data for an Al sample ($1.5 \times 0.8 \times 0.3$ cm) is shown in Figure 3 taken with the set-up of Figure 1. The scan shows transmitted amplitudes as a function of position along the sample length with the minimum signal corresponding to a position of laser absorption directly above the edge hole. For comparison the same sample is shown with the laser replaced by a second 10 MHz transducer, Figure 4, serving as the ultrasonic generator. Here, most of the detail of signal of Figure 3 is lost due mainly to the large transducer diameter compared to the flaw diameter. The comparison illustrates a major advantage of the laser technique; i.e., in other words the ability to produce sufficiently small acoustic beams in order to image closely spaced submillimeter defects.

A similar set of data for a Ti sample containing edge through-hole defects is shown in Figure 5. We have also obtained data using two 10 MHz detectors which again show much poorer resolution than that obtained with the laser.

In addition to through hole and edge hole detection we have also attempted to detect the presence of cracks in samples of steel and stainless steel in the thickness range 0.005 to 1 cm. To simulate cracks in these samples, electron discharge milling (EDM) was employed at the suggestion of W. Scott of (NADC) the Naval Air Development Center. Resulting EDM slots were $\sim 0.002-0.004$ cm wide, 0.002 cm deep and ~ 0.1 cm in length. For all samples tested with the crack submerged (clamped) in water but facing the incident laser source, a clear ultrasonic indication was obtained by the change in the transmission amplitude detected at 10 MHz when scanning over the crack. However, we were not able to obtain definitive

evidence of the crack when the EDM slot was facing away (i.e. smooth surface facing laser) from the laser beam. Thus the ability to find hidden flaws of this dimension appears to be difficult if not impossible at 10 MHz. Further investigations are warranted to determine whether the present scheme might be useful in finding hidden cracks using detectors tuned to higher frequencies. Immersion detectors are presently available up to 50 MHz (Panametrics) but we have so far not had them available for our experiments.

2. Thin Films

Differences in film thicknesses have been detected using the set-up described in the previous paragraph with detection at 20 MHz. The samples consisted of copper lines ~ 5μ high with widths varying between 15 – 500μ. The lines were deposited on a 500 Å background metallization consisting of copper-chrome. These lines were readily distinguishable from the background metallization by both optical and thermoelastic inspection so long as the lines were facing the incident optical radiation. Examples of detection at 20 MHz are shown in Fig. 6 for the lines facing the incident radiation. The presence of the lines is indicated by an increase in transmitted signal due apparently to a greater absorption of the incident radiation. However, with the sample inverted so that the lines were effectively "blind", it was not possible to obtain a clear difference in acoustic signal between lines and background. It is likely that for micron sized flaws, photoacoustic techniques as described by Rosencwaig et al[4] and Luukkala et al[5] would be more effective since a longer thermal wavelength would probe the samples below the surface more effectively than that resulting from the short pulses (nsec) of laser radiation.

3. Graphite-Epoxy

One sample of graphite-epoxy was supplied by NADC which was sectioned into smaller pieces in order to fit the water tank shown in Figure 1. For the section under test, one lamination had been removed so that a hole existed over an ~ 1.5 cm region. Data for this section is shown in Figure 7, taken by having the laser absorbed directly by the submerged sample, using water as the clamp 7a and interposing a rubber membrane to act as the optical

absorber and elastic wave generator, Figure 7b. We interpret the fluctuation in amplitude of the received signal as being due to the bonding material filling in the graphite-epoxy defect nonuniformly. Similar, though considerably less detailed fluctuations in the received signal were obtained with the use of a second 10 MHz transducer to replace the laser elastic wave generation, Figure 8. It is therefore quite clear that laser generated thermoelastic waves can readily detect hidden flaws in graphite-epoxy. The resolution of this technique as it applies to this material remains to be determined.

4. Large Bulk Samples

Attempts to locate blind cracks in turbine blades (supplied by NADC) using laser generated thermoelastic waves were not successful. For these experiments a 10 MHz immersion transducer in a water tank was used in conjunction with a frequency doubled Nd-YAG laser. This laser provided pulses of ~ 30 nsec half width at 5300 Å. Water served to clamp the complicated turbine blade surfaces in order to provide maximum optical to mechanical conversion efficiency. In an attempt to locate the internal cracks we were dependent on an approximate flaw location map provided by NADC. The received signals traversing the turbine ribs were not noticeably different as the laser was scanned along sections allegedly containing these flaws.

Conclusions

Hidden flaws, ~ 150 μ or greater in at least 2 dimensions have been found using laser generated thermoelastic waves both in the present work as well as some of the work already published.[1,2] Hidden flaws in the 1 – 25μ range in one dimensions such as cracks have so far not been detected by thermoelastic schemes. To detect such small flaws may require the following refinements; 1) higher detector frequency response; 2) a fast Fourier transform method to provide frequency rather than real time information from the received signal; 3) the use of photoacoustic techniques such as those described in Ref. 4 and 5 and in Section V.

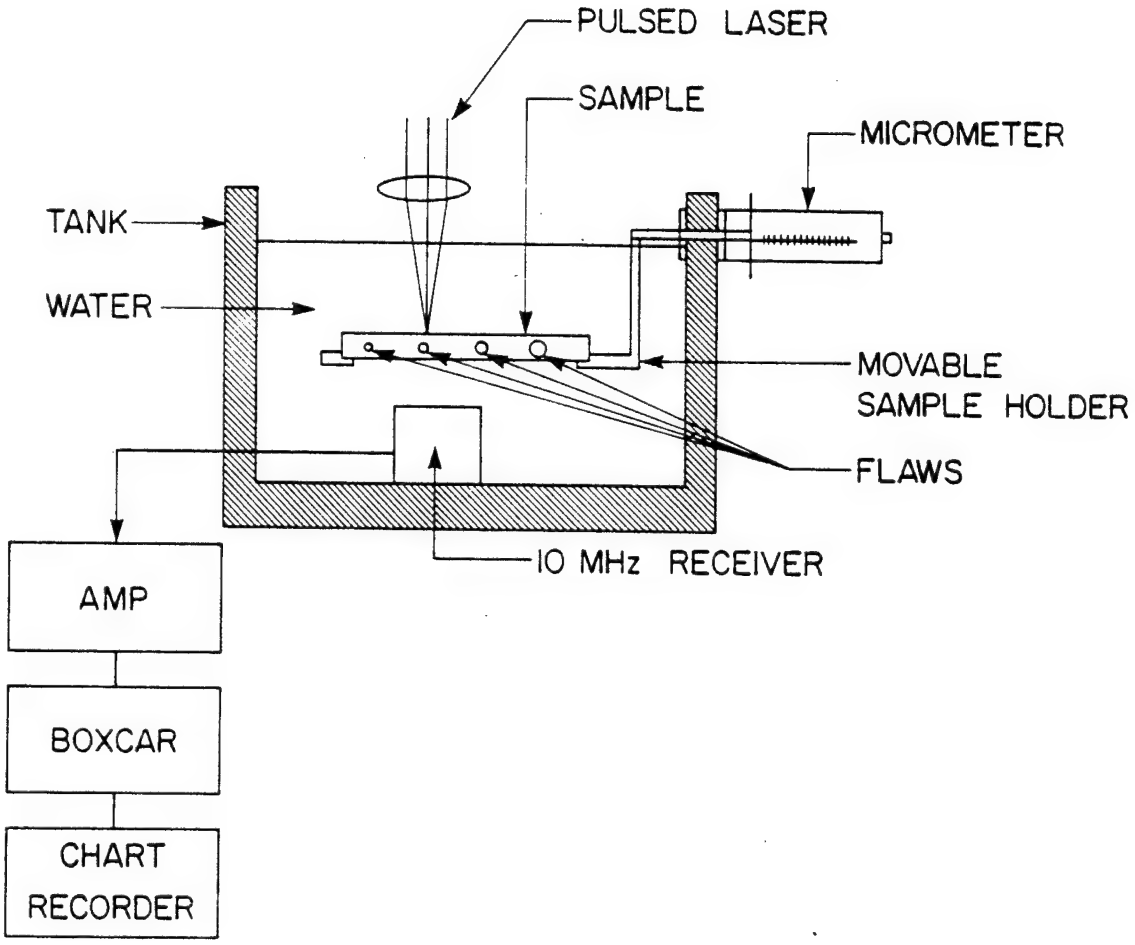

Fig. 1 Microscope stage water tank for flaw detection in transmission of water immersed samples.

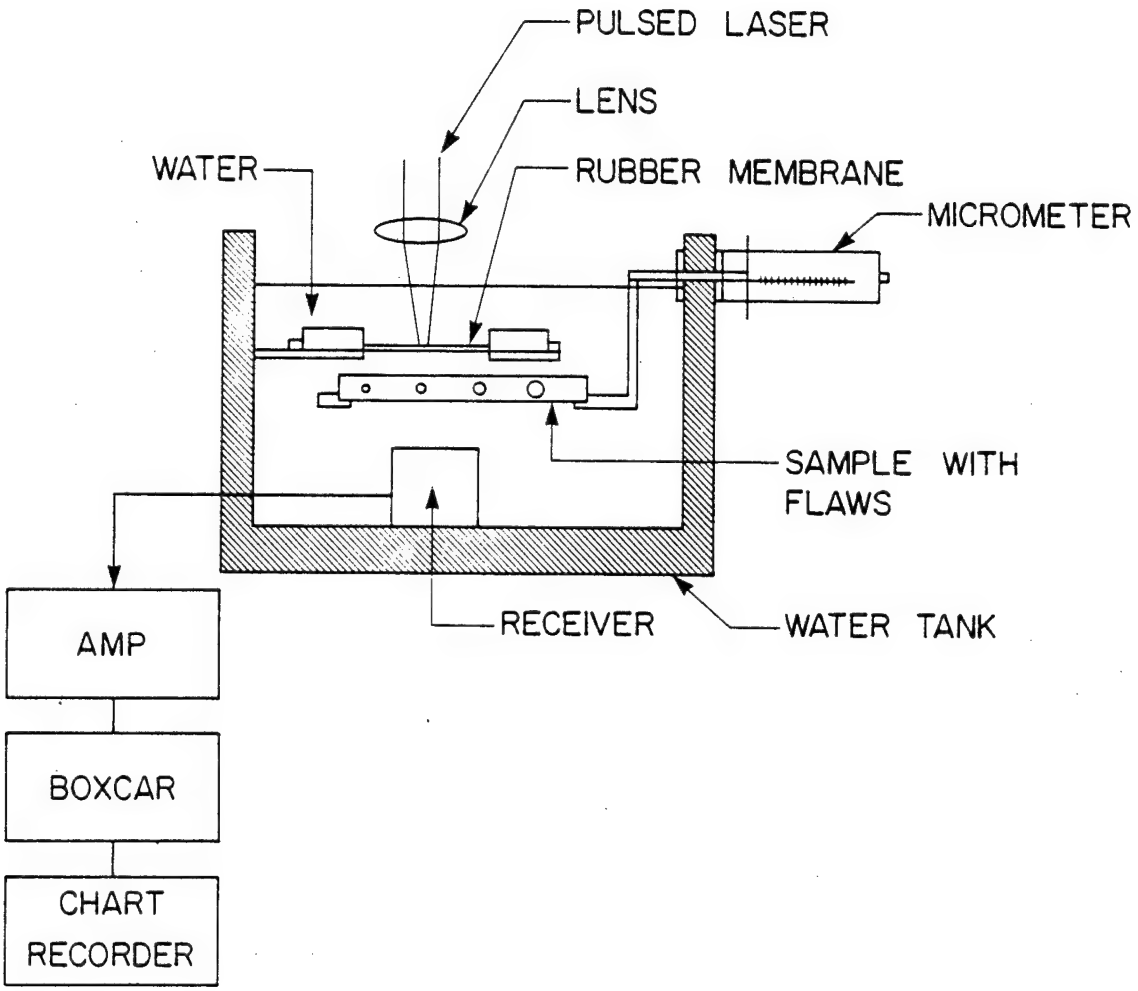

Fig. 2 Set-up for using rubber-water interface for laser generated elastic waves.

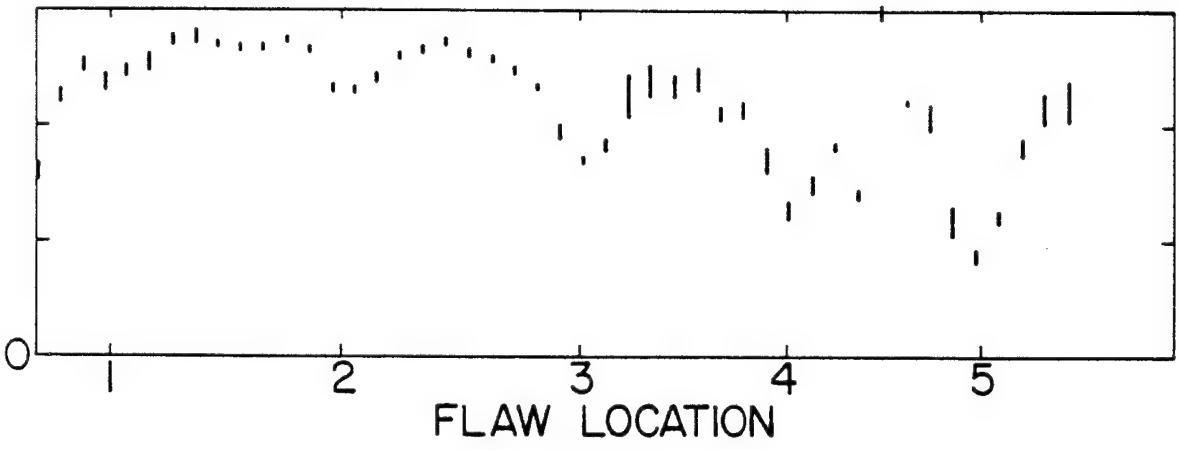

Fig. 3 Flaws in an Al sample using laser generated elastic waves.

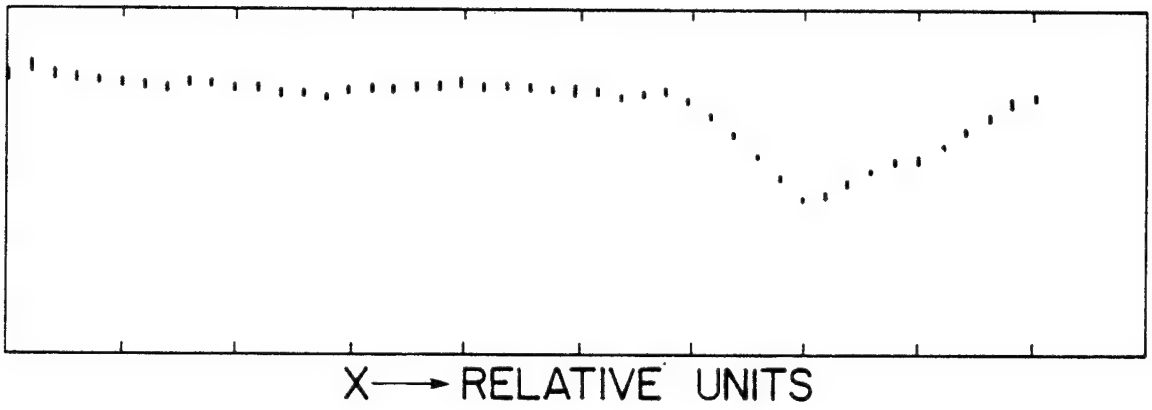

Fig. 4 Flaws in an Al sample using two piezoelectric transducers.

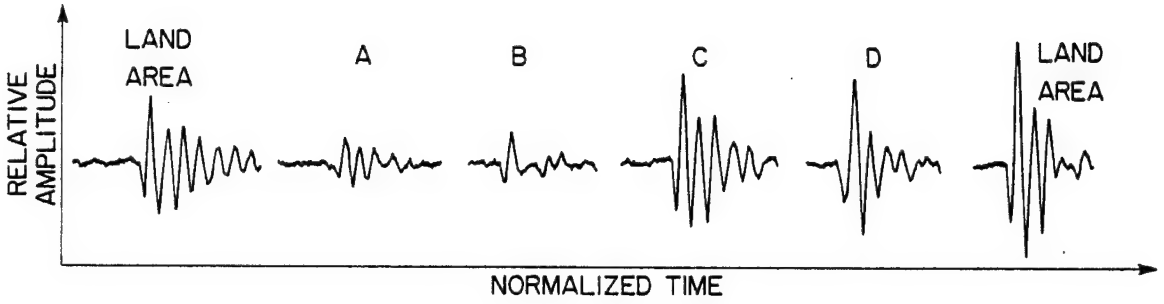

Fig. 5 Flaws in a Ti sample.

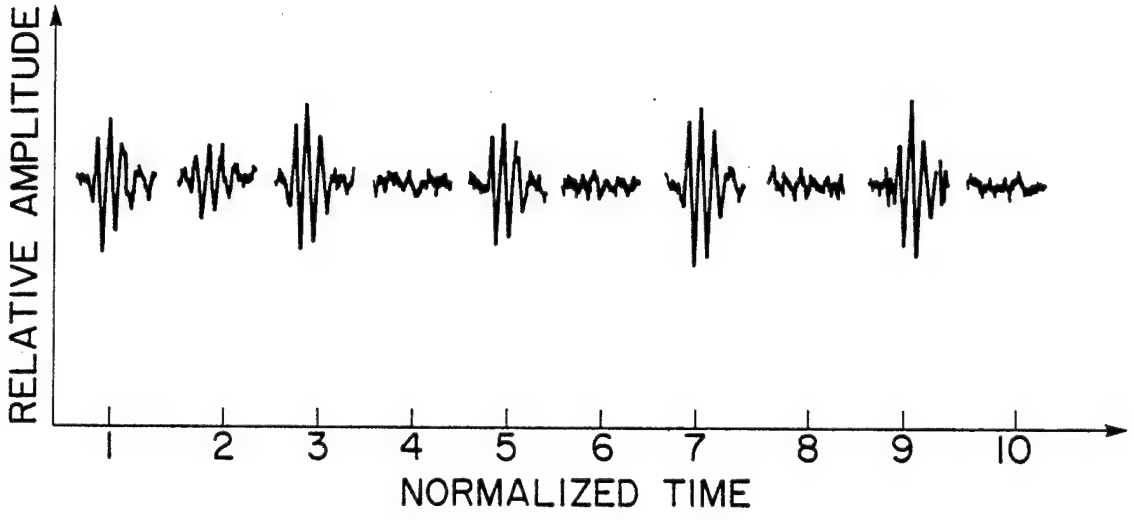

Fig. 6 Detection at 10 MHz of various thin film thicknesses deposited on glass.

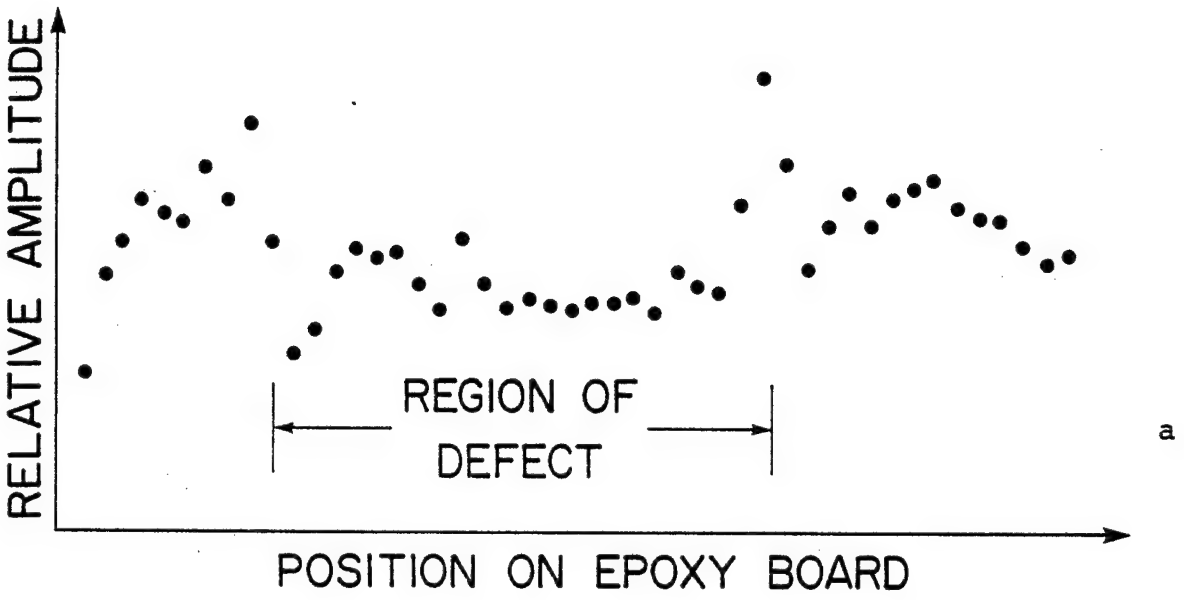

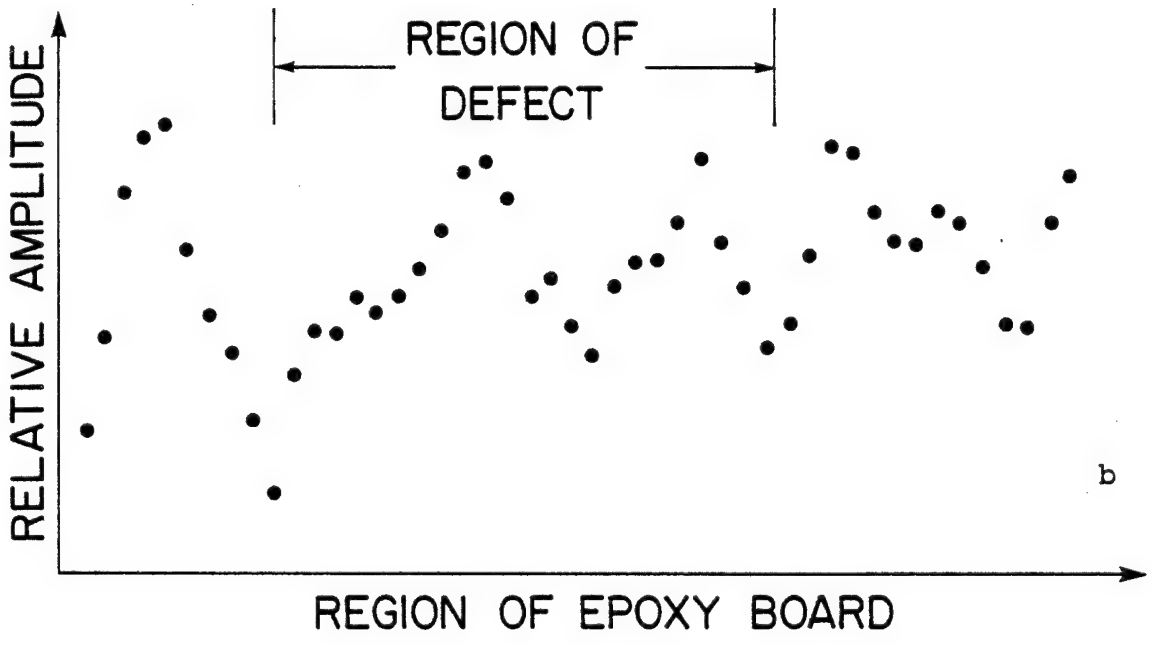

Fig. 7 Graphite-epoxy flaw detection using laser generation.

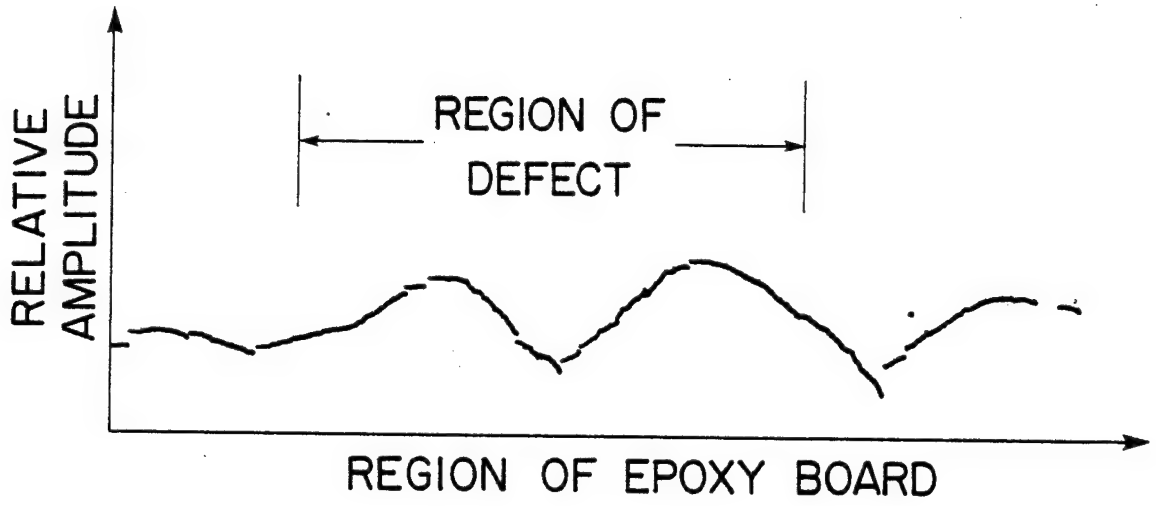

Fig. 8 Graphite-epoxy flaw detection using piezoelectric generation and detection.

this page purposely left blank

II. THERMAL PROFILES

In order to use lasers for non-destructive testing, it is important to know what limitations are required on the optical power density, pulse duration and repetition rate in order 1) to prevent damage to the absorbing material and 2) to prevent non-linear effects such as occur when water used as a clamp boils or cavitates. These considerations have led us to investigate (in collaboration with H. F. Budd) various thermal models in order to determine temperature/time profiles resulting from laser absorption. In all cases we have assumed an infinite absorption constant for the laser absorbing medium; in other words, i.e. surface absorption which is a good approximation for most metallic absorbers. A computer program has been set up for each of these thermal models in which approximations to the experimental conditions are made. The simplest of these three is for 1 dimensional heat flow for a 3 layered structure. Here, incident laser power passes through the first medium (clamping plate) without attenuation and is absorbed by the second medium consisting of a thin evaporated layer. This layer is in contact with a third medium, semi-infinite in extent. This structure has been previously described in conjunction with the generation of elastic waves at a solid-liquid interface.[6] Solutions for several special cases of the temperature-time profiles of such a structure are shown in Fig. 9 for an absorbed power density of 1 W/cm^2. Figure 9 includes values of the temperature for the clamped case, glass-Au-α-quartz as well as the unclamped case; in other words, i.e. where medium 1 is taken to be air rather than glass. The removal of the clamp becomes relatively unimportant on the temperature maximum for shorter laser pulse widths although the effect on the elastic amplitude is greatly effected as previously shown.[6] For this structure, power densities as high as 10^6 W/cm^2 can be used without causing damage with 10 nsec pulse widths based on the results shown in Fig. 9. It is important to observe the relatively long temperature decay time for each applied pulse. For sufficiently short pulse widths and slow repetition rates this decay can be shown to approach the initial ambient temperature. This is not true in general, however, and we are presently working on the 3

dimensional heat flow case for a continuous periodic train of pulses. This calculation is not yet complete.

We have also modeled the 3 medium single pulse case for 3 dimensional heat flow for an incident laser pulse of arbitrary gaussian radius, r_o. A comparison between 1 dimensional and 3 dimensional heat flow is shown for a glass-Au-α-quartz structure in Figure 10 with $r_o = 5\times10^{-3}$ cm, Au thickness = 2×10^{-5} cm a power density of 1 W/cm^2 at the center r = 0 and a pulse width of 1 μsec. The power density for the 1 dimensional case is also 1 W/cm^2 Not surprisingly, the heating portions for the two cases are essentially identical since very little lateral heat spread can occur in 1 μsec in these media. The curves begin to deviate from one another at ~ 3 μsec. It is clear that for long pulse widths the 1 dimensional calculation cannot be used since the peak temperature will be overestimated while the cooling rates will be underestimated. However the case of three dimensional heat flow for a single pulse is a good approximation from which the maximum temperature can be estimated for the low repetition rates used in our experiments.

In Figure 11 we include calculations for two media structures which can be used to approximate the conditions of the experiments on flaw detection in bulk samples using water as the clamping material (see Section I, Flaw Detection). In the limit of a very thin layer for medium[1] and long pulse lengths, exact solutions for the temperature profiles can be derived from the homogeneous medium solutions found in Pittaway.[7] In the computer solutions of Fig. 11, the water layer and the sample dimensions are considered large compared to thermal diffusion lengths $2\sqrt{kt_o}$ when k is the thermal diffusivity and t_o the incident pulse width. From these curves we determine that for water-Al and water-steel interfaces, 5 nsec pulses of up to ~ 10^6 W/cm^2 can be absorbed without causing the water to boil. This sets the limiting temperature for maintaining linearity of the detected acoustic signal. Any boiling or cavitation of the liquid results both in nonlinear behavior as well as noisy output signals.

Experimentally, values of laser power density that were below damage threshold, either to the sample or the clamping layer, were found to be in the range ~ 10^5 to 10^7 W/cm^2

for pulse repetition rates on the order of 10 Hz with laser pulse widths on the order of 5- 30 nsec. This 2 orders of magnitude power density range includes the large variety of bulk and thin film samples we investigated and described in the previous section. In order to determine the limiting power density values more precisely one requires knowledge of the thermal parameters and dimensions of all the materials of the thermoelastic generating structure as well as the solutions to the 3 dimensional heat flow problem.

In general it is clear that flaw detection can be accomplished using thermoelastic expansions to generate elastic waves without damage to the test sample. The extent to which signal averaging is necessary together with the required data rate will determine the allowable incident peak laser power density below damage threshold. Whether laser generated elastic wave detection is practical with the above limitations also depends on the specific thermal and elastic parameters of the particular material under study.

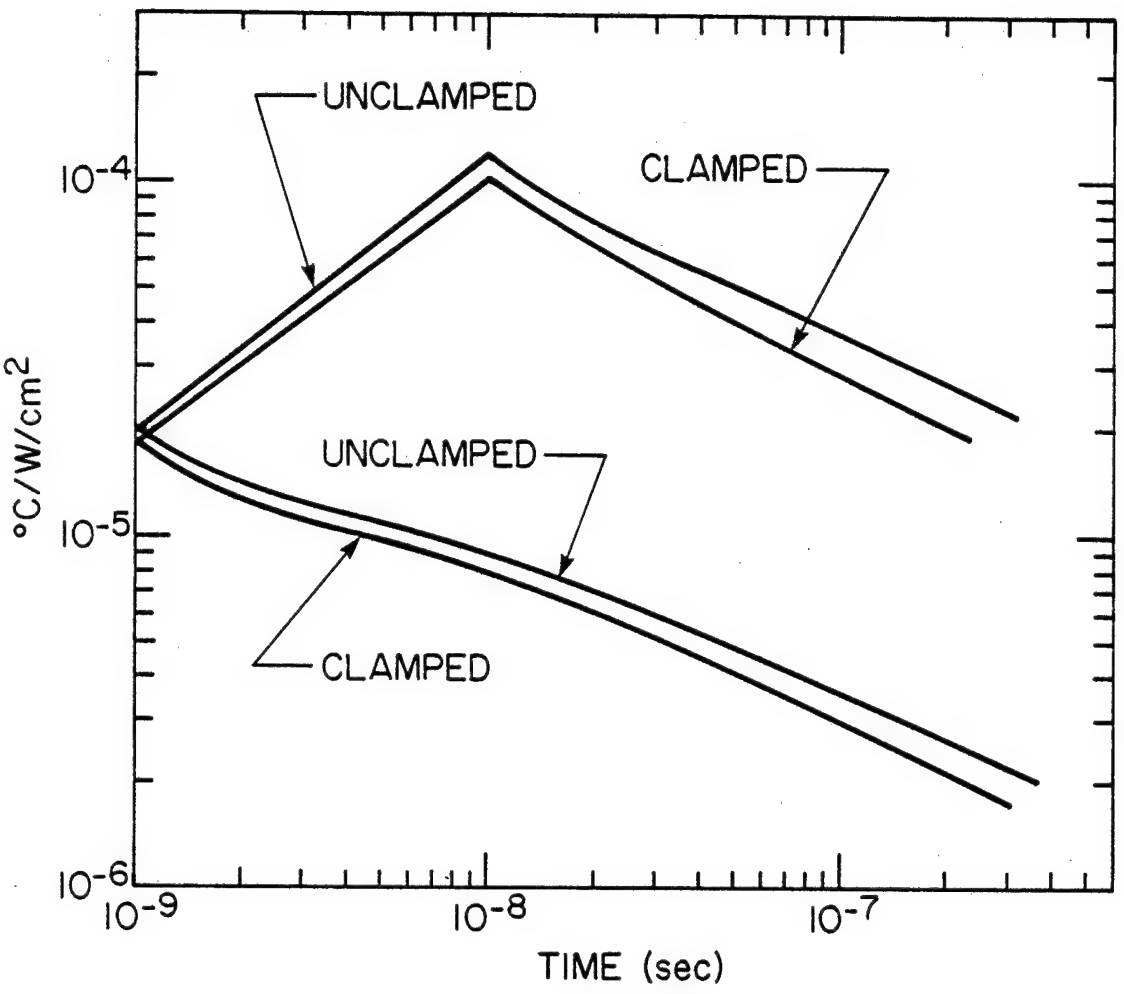

Fig. 9 Temperature-time profile for a glass – Au – α – quartz structure.

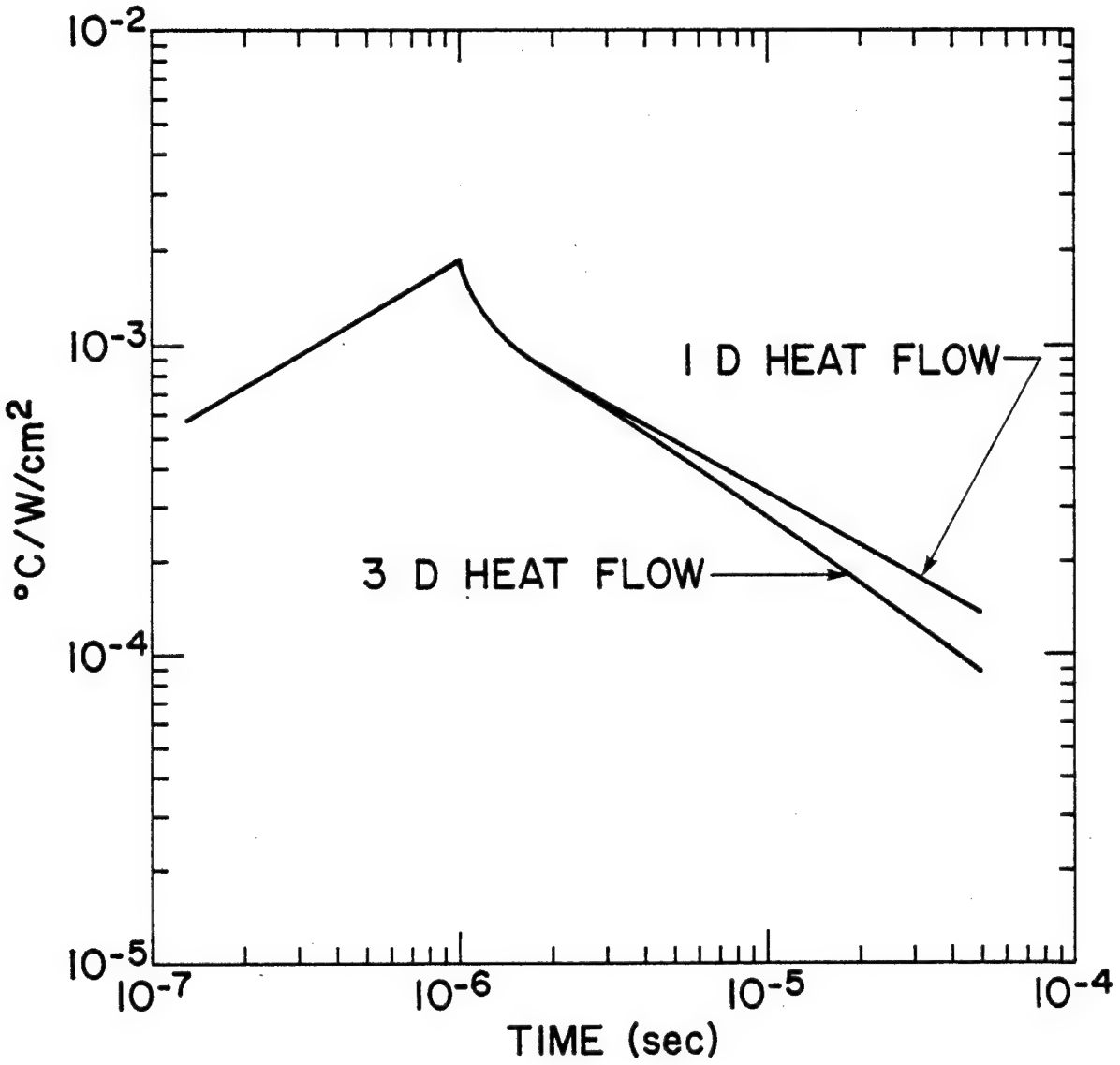

Fig. 10 Temperature-time profiling comparing 1 and 3 dimensional heat flow.

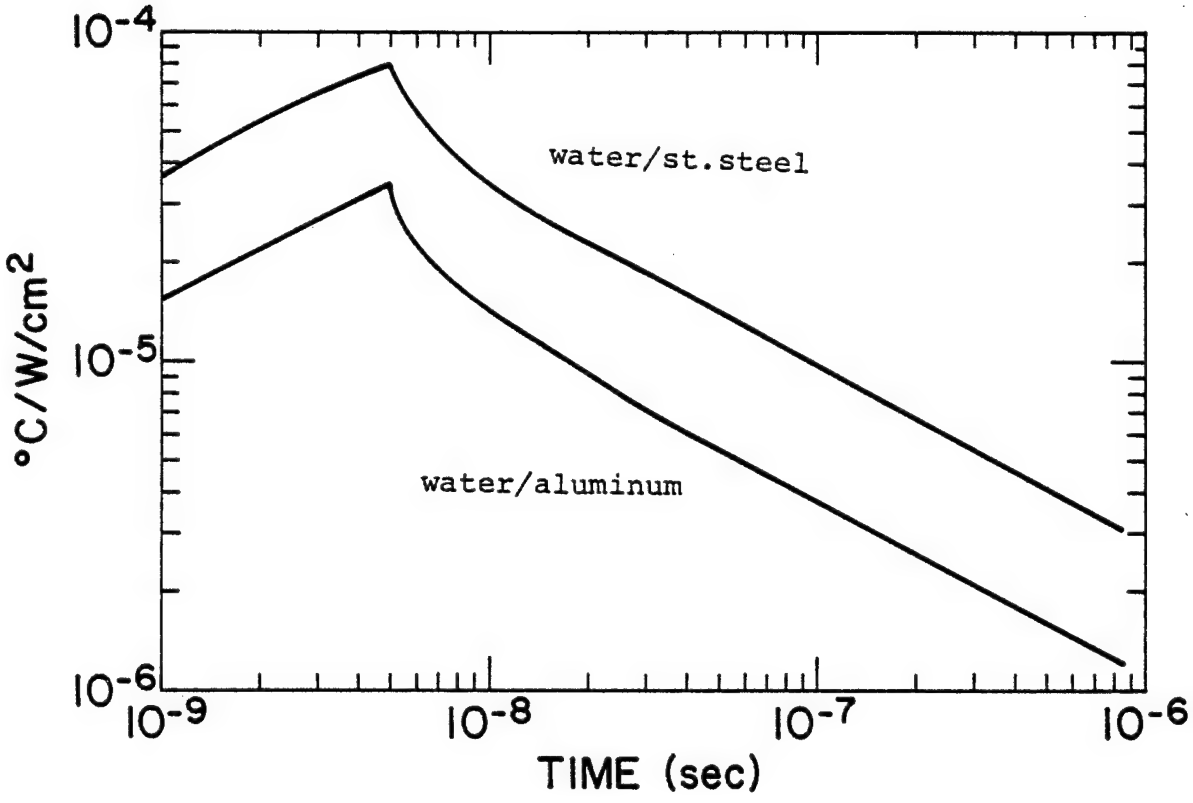

Fig. 11 Thermal profiles from gaussian laser beam irradiation.

III. LASER GENERATED THERMOELASTIC BEAM PROFILING

The purpose of this investigation was to determine the acoustic radiation pattern in water emanating from a thin film of tungsten on glass upon the absorption of pulsed laser radiation. In our experiments 2.5×10^{-2} cm glass slides with 2000 Å thick films, e-beam evaporated, were mounted vertically on the inside transparent wall of a water tank with the film's free surface facing into the water. An Nd-YAG frequency doubled laser (5300 Å) was directed through the wall and absorbed by the film at the glass-film interface, exciting a spot ~ 2 mm in diameter. The laser was operated at ~ 6 kW output with a mode pattern that was approximately gaussian. The elastic wave resulting from the 30 nsec wide pulses propagates from the heated film into the water as well as into the tank wall. However, these two waves are easily distinguishable by their difference in arrival time at the receiver, in this case a 6 mm diameter, 10 MHz Aerotech immersion transducer. The receiver was mounted on a precision arm capable of x, y motion either by manual or motor drive, the latter controlled by a microprocessor. The z direction was manually adjustable. The experimental arrangement is shown in Figure 12. The system includes the capability for digitizing the detector signal using an on-line computer; however, for our experiments this option was not utilized. Rather, the detector amplitudes were recorded manually from an oscilloscope as a function of receiver position. Computer graphics were used to generate a display of amplitude in a given x, y plane.

A typical radiation field for the plane z=0 where z is measured from the center of the laser absorption spot is shown in Figure 13. Here the amplitude falls off with distance from the source while spreading laterally as expected from simple diffraction theory. In the far field pattern; in other words, $x >> \lambda$ a simple comparison to Fraunhofer diffraction is useful[8], where for a circular source the amplitude U is related to the first order Bessel function J_1,

$$U \propto \frac{2J_1(kaw)}{kaw} \tag{1}$$

where **a** is the radius of the aperture (laser spot), $k = \frac{2\pi}{\lambda}$ with λ the wavelength in water at 10 MHz, $W = \sin\theta$ with θ defined by the angle between the x axis and distance from the origin to the point on the diffraction pattern. Secondary maxima in the diffraction pattern are predicted to be much smaller than the primary peak and are also not observed experimentally. From the tabulated values in Reference 8, the first zero value for equation (1) occurs at kaw $= 1.2\pi$. This yields the well known result for diffraction from a disk,

$$w = \frac{1.2\lambda}{a} \tag{2}$$

and gives for our 10 MHz waves for a spot ~ 1 mm in radius

$$\sin\theta = 1.8\times10^{-1} \tag{3}$$

At a distance of 178 mm from the source (Figure 13) the first zero corresponds to $\sin\theta = 5\times10^{-2}$. This smaller-than-predicted observed diffraction angle can be due to the following causes: 1) an underestimate of our laser spot diameter 2) the nonuniformity of the power density of the spot 3) errors in the detected signal due to phase cancellation across the face of the detector. We have on several occasions attempted to reduce these cancellation effects by means of specially designed aperture plates to limit the active area of the receiver, however these results will not be further discussed here.

In Figure 13 the change in area under the amplitude curves as a function of x can be accounted for almost exclusively by the amplitude attenuation of water at 10 MHz, 0.029/cm.

In addition to the laser generated elastic beam profiling, we have also tested several thin films using electrical pulse heating rather than lasers to generate thermoelastic waves. In these cases it was relatively easy to vary the generated elastic center frequency by varying the pulse width of the pulse generator. Several diffraction patterns for these films have been recorded and also found to obey the simple Fraunhofer diffraction rules.

Thus we have shown that it is relatively simple to utilize thermoelastic expansions to generate collimated beams which can be used for material flaw or medical diagnostic purposes. Since there is no need for special bonding or backing techniques for the excitation element as

is typical for piezoelectric materials it is not surprising that a well collimated elastic beam results from thermoelastic expansions, as predicted from a simple piston model[9] in conjunction with Fraunhofer diffraction theory.

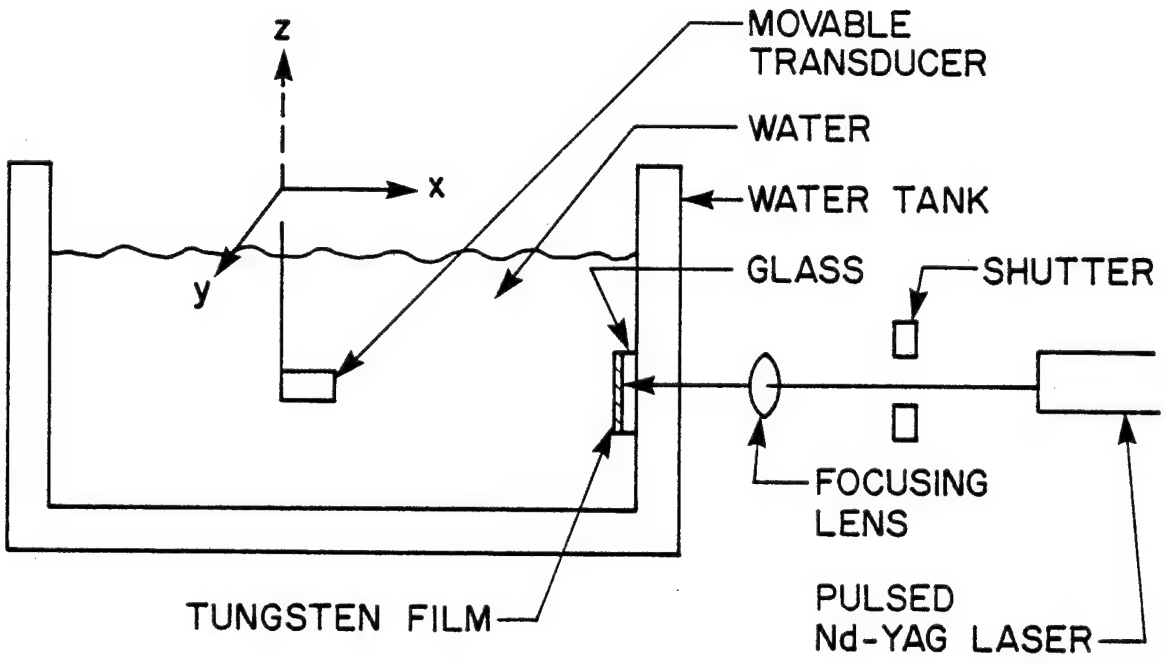

Fig. 12 Beam profiling water tank and schematic.

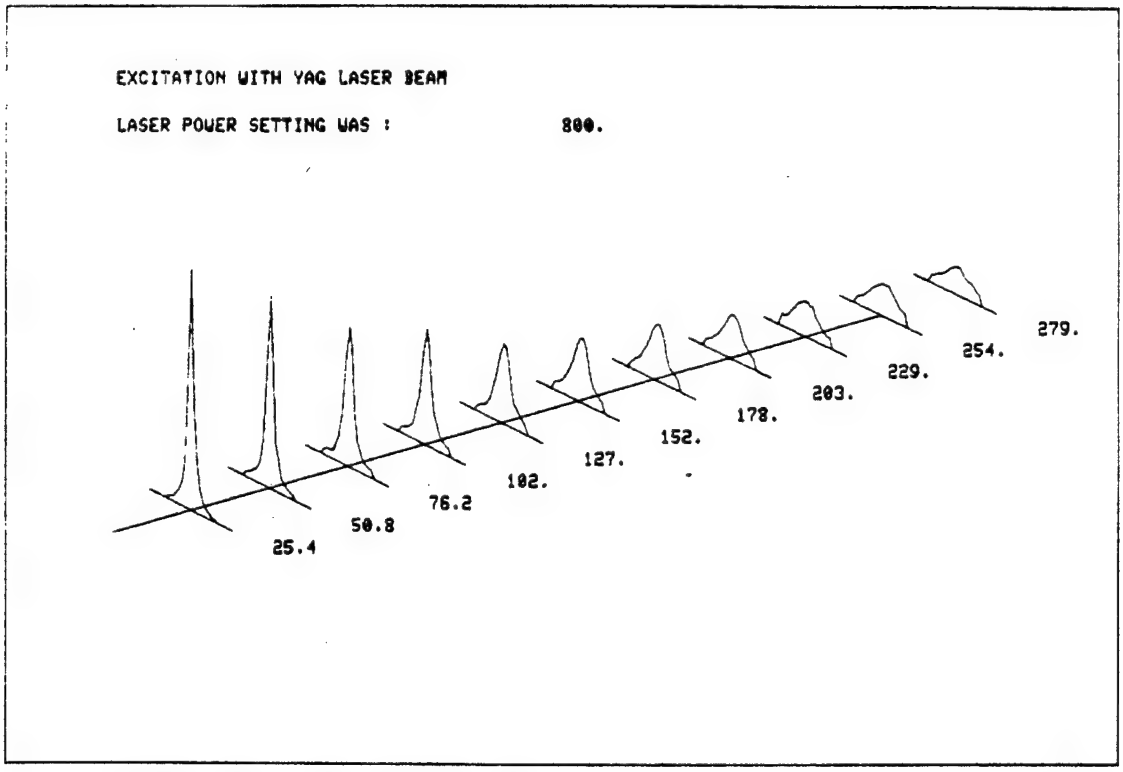

Fig. 13 Computer graphics of laser generated acoustic beam.

IV. THERMOELASTIC EFFECIENCY

Theory

The efficiency of the conversion of optical energy to elastic energy is an important parameter in evaluating the effectiveness of thermoelastic wave generation. White[9] has devised a simple 1 dimensional theory for the conversion efficiency of incident harmonically varying radiation absorbed by an unclamped surface. We have applied this theory to pulse heating of clamped surfaces with the following approximations: (1) our 3 layered structure can be treated like a homogeneous medium, (2) the harmonic variation is derived from the Fourier components of the incident pulse, (3) the relevant terms of the Fourier expansion are determined by the bandwidth of the receiver. For an optical flux F (w/cm^2) varying with angular frequency ω as,

$$F = F_o \cos \omega t \tag{4}$$

the expression for the conversion efficiency η of a homogeneous clamped medium because,

$$|\eta| = \frac{5.7 \times 10^{-9} v \beta^2 F_o}{\rho C^2} \tag{5}$$

where v is the acoustic velocity (cm/sec) β the linear thermal expansion coefficient, ρ the density (gm/cm^3) and C the heat capacity (cal/gm). It is interesting to note the dependence of η on the incident flux, F_o. Theoretically the efficiency could reach 100% except that the fluxes required would produce non-linear deviations from the simple theory and more likely melting of the material even for values of F_o considerably below the theoretical 100% efficiency value.

Values of η/F_o for clamped homogeneous materials are listed in Table I derived from equation (5). It is important to recognize that in general more than 1 medium is required to realize the clamped condition so that the values in Table I are upper limits. In a previous paper we have calculated the strain/watt/cm^2 absorbed power for a 3 layer structure.[6] We have used these strain values to calculate η for the structures listed in Table II. Here a

relatively large efficiency is obtained by utilizing the high expansion coefficient of a liquid. These values were obtained from a computer program which solved both the 1 dimensional heat flow and the coupled elastic wave equation for the 3 media. For details of strain as a function of the thickness of medium 2 the reader should refer to Reference 6.

It is especially interesting to note the large value of η predicted for liquid **He**. This gives rise to the possibility of generating large elastic amplitudes in low temperature environments.[10] Alternatively, if liquid **He** itself is not the generating medium, the decreasing heat capacity with lower temperatures gives rise to increasing conversion efficiences. A possible application of this effect is the laser generated elastic waves for NDT at low temperatures, for example Josephson devices at liquid helium temperatures.

The efficiency of thermoelastically generated waves is generally orders of magnitude less than that obtainable from PZT. The latter has under optimum circumstances, yielded efficiencies well over 30%.[11] This is physically unrealizable thermoelastically. In our experiments with incident power densities on the order of 10^5-10^6 w/cm^2 efficiencies on the order of 10^{-7} result. It is important to realize however that the advantage of laser generated thermoelastic waves lies in the flexibility both for scanning and probing very small regions in order to provide high resolution detection of flaws. A particular advantage of the laser technique is the ability to probe materials with complicated or irregular surface contours not readily amenable to investigation with standard transducers. On the other hand, for those cases where high conversion efficiencies are an important consideration, thermoelastic generation will not be a viable technique for NDT.

Sample Calculation and Experimental Comparison

We refer now to the apparatus of Figure 1 and perform an approximate sample calculation for the expected acoustic power generated at the surface of a titanium sample. We assume the sample to be clamped by water, and the excitation source to be a 5 nsec laser pulse with power absorption over an area 2×10^{-5} cm^2 (total absorbed power is 50 W). This corresponds to the conditions shown in the data of Figure 5 in regions away from the flaw.

We use equation (5) to determine the efficiency, η, and acoustic power expected for the absorbed power density of $\sim 2.5 \times 10^6$ W/cm^2. The following corrections are required to determine the acoustic power expected at the transducer (assumed matched to water); 1) a power reflection loss $\left(\frac{4z_1 z_2}{(z_1 + z_2)^2} \right)$ where z_1 and z_2 are the acoustic impedance of Ti and water respectively and a bandwidth correction. This latter correction comes about due to the fact that the acoustic spectrum extends from 0 to approximately 200 MHz for a 5 nsec pulse excitation. The bandwidth of our receiver is $\pm$ 25% of the center frequency so that 5/200 of the available bandwidth is detected, i.e. 2.5×10^{-2}. Thus, with these corrections applied to the thermal and elastic parameters substituted in equation (5), we obtain a value of the acoustic power equal to $\sim 2.3 \times 10^{-6}$.

This value has to be compared to the observed signal from the Aerotech Model transducer across 50 Ω which is observed to be $\pm$ 20 mV after 40 db of gain. Thus the approximate electrical power for such laser excitation is 8×10^{-10} W after correction for the preamp. Correction for the one way insertion loss (given as 32 dB by Aerotech for pulsed excitation) implies that acoustic power for this excitation is 1.3×10^{-6} W. This close agreement between experiment and calculation (i.e. the 2.3×10^{-6} W above) should not be taken too literally due to a number of very gross approximations in the theory and experimental corrections. However, the results give a good order of magnitude type comparison which in this particular example gives very close agreement.

Table I

Material	ηF_o
fused quartz	1.2×10^{-12}
pryex	1.2×10^{-14}
Mo	2.1×10^{-12}
water	5.3×10^{-12}
acetone	7.6×10^{-10}
liquid He (4.2°K)	$\sim 1 \times 10^{-5}$

Conversion efficiency to elastic power/w/cm^2 absorbed optical power for a clamped homogeneous medium based on equation (5).

Table II

3 Layer Configuration [(Limit as $\tau d \rightarrow o$]	η/F_o
pyrex – Mo-acetone	$\sim 8 \times 10^{-11}$
pyrex – Mo-method	$\sim 4 \times 10^{-11}$
pyrex – Mo-water	$\sim 1 \times 10^{-12}$

Conversion efficiency (elastic power/unit absorbed power/cm^2) for a 1 dimensional computer solution for a 3 layered structure. For details of the calculation refer to reference 6.

V. PHOTOACOUSTICS

INTRODUCTION

We have made a variety of preliminary photoacoustic measurements with a number of different cell configurations to study the merits of this technique for possible use in material flaw detection. Our data enable us to make some qualitative comparisons to the pulsed laser techniques already described.

Two types of photoacoustic cells were investigated consisting of a closed cell with the sample forming one end of the cell. In one case a miniature microphone was used to detect the modulated pressure wave, a system similar to that described by Tam and Wong.[12] In an alternate configuration, a PZT hydrophone was used in place of the microphone, with the cell again forming a closed system, water replacing the air volume and the sample attached to the opposite end of the cell. Two types of PZT detectors were used, one modeled after Patel and Tam,[13]. the other utilizing a cylindrical PZT element. The latter cell has been used in conjunction with an operational amplifier resulting in a signal to noise figure of ~ 1000:1. Thus, with incident power on the order of only 100 mW (absorption in the sample on the order of 50%) signals on the order of 10–50 mV are obtained with modulation frequencies in the range 10^2–10^3 Hz.

THEORY AND EXPERIMENT

Thermal wave imaging has been described by several investigators as a means of flaw detection.[4,5, 12-14] The thermal wavelength, μ, is intermediate in length to that typical for standard photoacoustics and that representative for thermoelastic waves generated by submicrosecond pulses.[1,2]. Here μ is defined by

$$\mu = \sqrt{\frac{2\kappa}{\omega}} \tag{6}$$

with ω the angular optical modulation frequency and κ the thermal diffusivity of the optically absorbing surface.

Our interest in photoacoustics stems from the recent reports on thermal wave imaging (where μ is sufficiently large to sample subsurface flaws) together with a particular approximate derivation for the oscillating pressure variation as a function of photoacoustic cell geometry found in Reference 12. This analysis has suggested the possibility of achieving very high signal as well as signal to noise ratio for thermal wave imaging by having the sample under investigation in contact with a liquid so long as the thermal wavelength extends well into the liquid. This "thermal leak" technique in which heat from a solid is transferred to a liquid with a relatively high thermal expansion coefficient has been previously described in conjunction with generating large thermoelastic amplitudes in thin films in contact with liqudis.[6]

An approximate theory for the microphone-air cell shown in Figure 14 is derived from the "piston" model of Reference 12 in terms of a local temperature-pressure-change, with the pressure communicated to the entire closed volume. For modulated optical radiation absorbed at the air-sample interface, a temperature change occurs in the volume determined by the laser beam of radius r and thermal diffusion length of the air, μ_g, so that a net pressure change occurs throughout the cell of radius R equal to

$$\delta P \approx \frac{\gamma P \mu_g \mu_s F_o r^2}{[K_s \ell_g T R^2]} \tag{7}$$

Here F_o is the absorbed laser flux, ℓ_g is the length of the cell, T, the absolute temperature, γ is the gas constant, μ_s the thermal diffusion length in the sample, K_s the sample thermal conductivity. We have here assumed zero residual volume in the microphone and $\ell_g > \mu_g$. Using this theory I have derived an expression for a cell similar to that of Figure 14 replacing the air with water and the microphone by a hydrophone. Here the local temperature change occurs in a volume equal to $\pi r^2 \mu_w$ where μ_w is the thermal diffusion length in water. The resulting pressure change communicated to the entire cell volume is,

$$\delta P \approx \frac{\rho v^2 \beta r^2 \mu_w \mu_s F_o}{K_s R^2 \ell_g} \tag{8}$$

with ρ and v the density and acoustic velocity of water. The advantage of the closed water cell over the air-cell is shown by taking the ratio of the respective oscillating pressure changes, given in Equations 7 and 8, a ratio equal approximately to 100 at room temperature.

In our initial experiments in photoacoustics we used an air-cell together with a Knowles 1754 microphone using stainless steel platelets as samples varying in thickness from 2–20 mils. Photoacoustic amplitudes were measured using either a CW krypton or argon laser mechanically chopped in the frequency range ~ 100–1000 Hz in conjunction with a PAR HR-8 lock-in detector. The cell was subsequently open and filled with water, the measurements repeated and compared to the air filled cell. An increase in signal by a factor ~ 6 was observed at around 170 Hz. As these microphones were not designed for use in water, it was not possible to continue these measurements before rapid deterioration in the detection sensitivity occurred. Subsequently, we used thin membranes to separate the water from the air space of the microphone. However, this arrangement introduces a relatively large microphone volume which substantially degrades the effect of the thermal leak into the water. Some increase in signal compared to an air-only cell was however observed.

The most promising modification of the photoacoustic water cell is shown in Figure 15 utilizing a cylindrical thickness polarized PZT element. This PZT cell has been used in conjunction with a 40 dB gain operational amplifier with signal to noise ratio at the output of ~ 1000:1. With incident laser power on the order of 100 mW (absorption of the stainless steel sample ~ 50%) signals on the order 10–50 mV are obtained for modulation frequencies in the range 100–1000 Hz. A plot of signal obtained with light incident on the air-sample surface for 2 mil, 10 mil and 16 mil stainless steel samples are shown in Figure 16. The frequency dependence is ~ $1/f^{3/4}$, consistent with Equation 8 for $\mu_s >$ sample thickness.

We are presently designing several thin samples with flaws to serve as "blind" defects to use in conjunction with this cell. So far successful flaw detection with this cell has consisted in detecting EDM slots (~ 2 × 2 × 40 mils) in 10 mil thick stainless steel with light

incident on the sample side containing the flaw. We have not yet detected this flaw "blind" but are continuing these experiments.

CONCLUSIONS

The photoacoustic technique appears to be applicable to flaw detection though somewhat less flexible than the submicrosecond laser pulse method in conjunction with using broadband detection. Disadvantages of the photoacoustic cells we have studied are the need for[1] small cell volumes and 2) the tight seal between sample and the cell medium (air or water). It would appear that for large or irregularly shaped samples this method would be hard to implement. On the other hand, small, thin samples could well be tested using this technique. Data rates might be relatively slow due to the sampling required for lock-in detection. It remains to be seen to what extent "blind" flaws can be detected with this method.

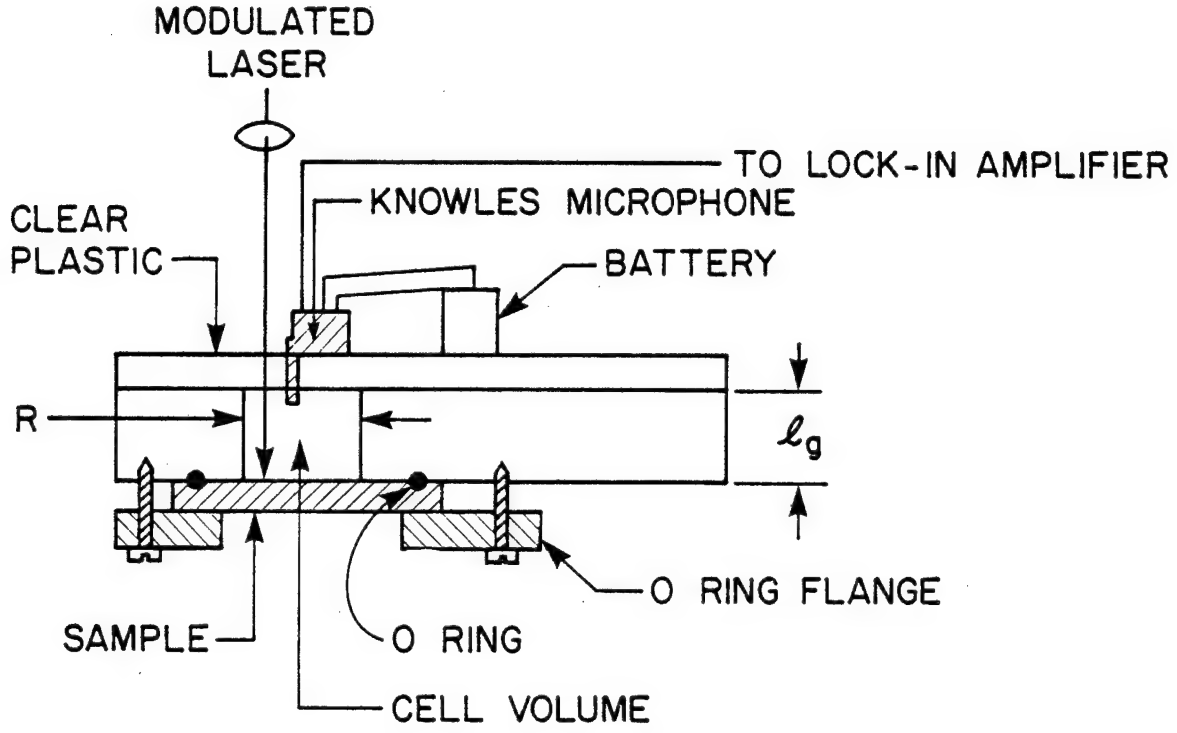

Fig. 14 Standard photoacoustic cell.

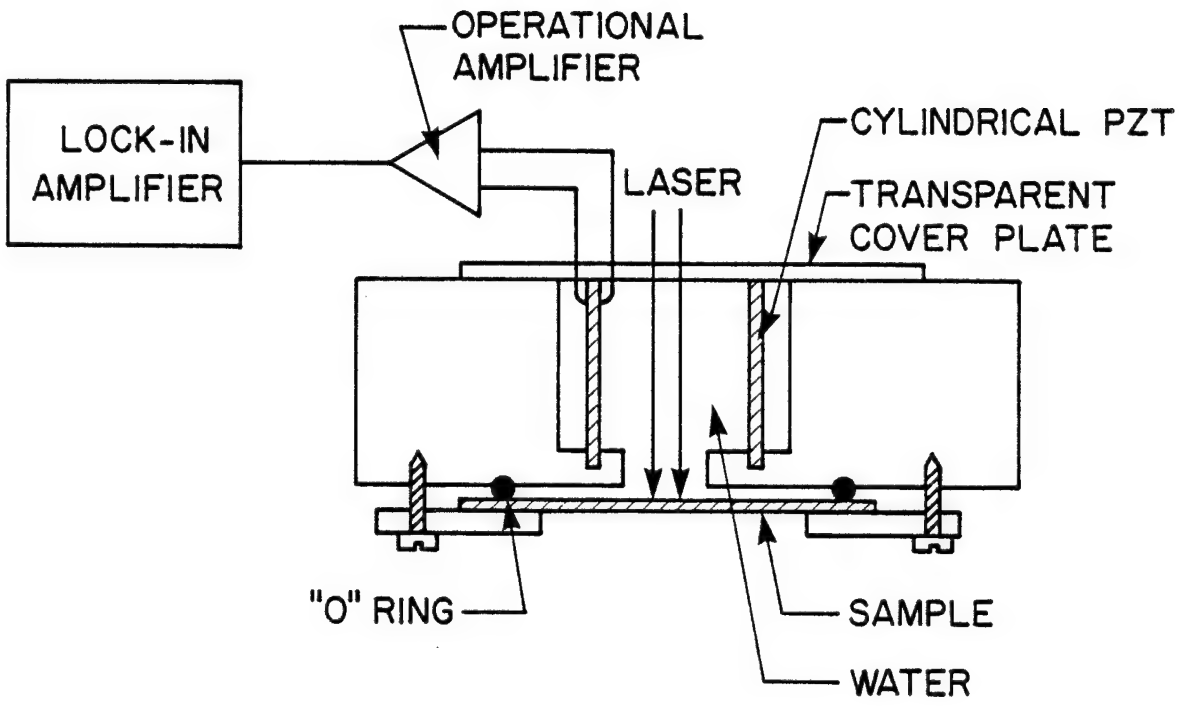

Fig. 15 Water filled photoacoustic cell.

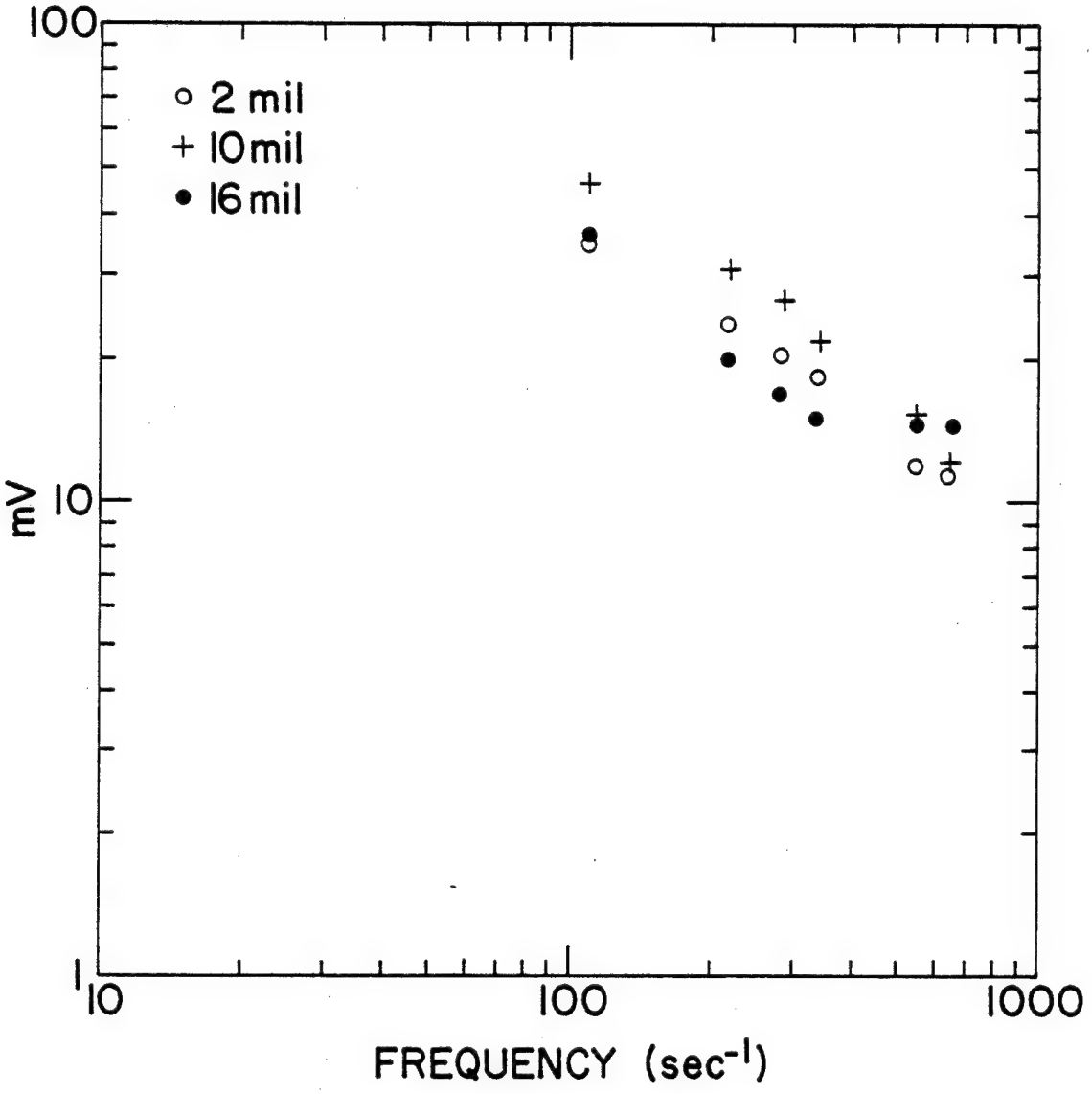

Fig. 16 Stainless-steel photoacoustic data.

VI. BIBLIOGRAPHY FOR LASER GENERATION OF STRESS WAVES IN LIQUIDS AND SOLIDS

O. K. Alekseeva, B. M. Zhiryakov, N. F. Popov and A. K. Fannibo, "Nature of Thermoelastic Stresses in Metallic Plates Subject to Laser Heating," Fiztkhim Obrab. Mater, (USSR) No. 5, 121 (1976).

N. C. Anderholm, "Laser Generated Stress Waves," Appl. Phys. Lett. 16, 113 (1970).

C. E. Bell and J. A. Landt, "Laser Induced High Pressure Shock Waves in Water," Appl. Phys. Lett. 10, 46 (1967).

C. E. Bell and B. S. Maccabee, "Shock Wave Generation in Air and in Water by CO_2 TEA Laser Radiation," Appl. Optics 13, 605 (1974).

F. V. Bernkin and V. M. Komissarov, "Optical Excitation of Sound Waves," Sov. Phys. Acoust. 19, 203 (1973).

A. I. Bozhkov and F. V. Bunkin, "Generation of Sound in a Liquid as a Result of Absorption of Modulated Laser Radiation," Sov. J. Quant. Electron. 5, 956 (1976).

M. J. Brienza and A. J. DeMaria, "Laser-Induced Microwave Sound by Surface Heating," Appl. Phys. Lett. 11, 44 (1967).

F. V. Bunkin, "Generation of Sound in a Liquid as a Result of Absorption of Modulated Laser Radiation," Sov. J. Quant. Electron. 5, 956 (1976).

G. Bushanam and F. S. Barnes, "Laser-Generated Thermoelastic Shock Wave in Liquids," J. Appl. Phys. 46, 2074 (1975).

J. C. Bushnell and D. T. McCloskey, "Thermoelastic Stress Production in Solids," J. Appl. Phys. 39, 5541 (1968).

G. Cachier, "Laser Excitation of Microwave Sound in Solids," J. Acoust. Soc. of America 49, 974 (1971).

C. A. Calder and W. W. Wilcox, "Noncontact Material Testing Using Laser Energy Deposition and Interferometry," Materials Evaluation 38, 86 (1980).

E. F. Carome, N. A. Clark and C. E. Moeller, "Generation of Acoustic Signals in Liquids by Ruby Laser-Induced Thermal Transients," Appl. Phys. Lett. 4, 95 (1964).

S. F. Cleary and P. E. Hamrick, "Laser Induced Acoustic Transients in the Mammalian Eye," J. Acost. Soc. of America 46, 1037 (1969).

D. C. Emmony, M. Siegrist and F. K. Kneubühl, "Laser-Induced Shock Waves in Liquids," Appl. Phys. Lett. 29, 547 (1976).

B. P. Fairand, A. H. Claner, R. G. Jung and B. A. Wilcox, "Quantitative Assessment of Laser-Induced Stress Waves Generated at Confined Surfaces," Appl. Phys. Lett. 25, 431 (1974).

B. P. Fairand and A. H. Claner, "Laser Generation of High Amplitude Stress Waves in Material," J. Appl. Phys. 50, 1497 (1979).

M. P. Felix, "Laser Generated Ultrasonic Beams," Rev. of Sci. Instr. 45, 1106 (1974).

M. P. Felix, "Distortion of Short-Duration Stress Pulses Propagating in Solids and Liquids," J. Acoust. Soc. of America, 58, 626 (1975).

J. A. Fox, "Effect of Water and Paint Coatings on Laser-Irradiated Targets," Appl. Phys. Lett 24, 461 (1974).

L. S. Gournay, "Conversion of Electromagnetic to Acoustic Energy by Surface Heating," J. Acoust. Soc. of America, 40, 1322 (1966).

W. F. Hartman, M. J. Forrestal and J. C. Bushnell, "An Experiment on Laser Generated Stress Waves in a Circular Elastic Ring," Trans. ASME 39, 119 (1972).

A. Karim and V. G. Velculescu, "On Laser-Induced Acoustic Waves in Non-Viscous Liquids," Rev. Rom. Phys. 23, 299 (1978).

S. G. Kasoev and L. M. Lyamshev, "Theory of Laser-Pulse Generation of Sound in a Liquid," Sov. Phys. Acoust. 23, 510 (1978).

Y. Kohanzadeh, J. R. Whinnery and M. M. Carroll, "Thermoelastic Waves Generated by Laser Beams of Low Power," J. Acoust. Soc. America 57, 67 (1975).

K. Kubota and Y. Nakatani, "Optical Excitation of Acoustic Pulse in Solids," Jap. Journ. of Appl. Phys., 12, 888 (1973).

M. Lax, "Temperature Rise Induced by a Laser Beam," J. Appl. Phys. 48, 3919 (1977).

R. E. Lee and R. M. White, "Excitation of Surface Elastic Waves by Transient Surface Heating," Appl. Phys. Lett. 12, 12 (1968).

Y. N. Lokhov, V. S. Mospanov and Y. D. Fiveiskii, "Thermoelastic Stresses Generated in Solid Transparent Dielectrics by a Focused Laser Beam," Kvantoraya Electron, (USSR) No. 3, 67 (1971).

T. J. Magee, R. A. Armistead and P. Krehl, "Laser Induced Stresses in Coated and Uncoated Targets," J. of Phys. D8, 498 (1975).

J. D. O'Keefe and C. H. Skeen, "Laser Induced Stress-Wave Impulse Augmentation," Appl. Phys. Lett. 21, 464 (1972).

M. W. Sigrist and F. K. Kneubühl, "Laser-Generated Stress Waves in Liquids," J. Acoust. Soc. of America 64, 1652 (1978).

M. W. Sigrist and F. K. Kneubühl, "Pressure Saturation of Laser-Generated Acoustic Waves in Liquids," Appl. Phys. Lett. 34, 353 (1979).

J. R. M. Viertl, "Frequency Spectrum of Laser Generated Ultrasonic Waves," J. Appl. Phys. 51, 805 (1980).

R. J. von Gutfeld and R. L. Melcher, "MHz Acoustic Waves from Pulsed Thermoelastic Expansion and their Application to Flaw Detection," Materials Evaluation 35, 97 (1977).

R. J. von Gutfeld and R. L. Melcher, "20 MHz Acoustic Waves from Pulsed Thermoelastic Expansions of Constrained Surfaces," Appl. Phys. Lett. 30, 257 (1977).

R. J. von Gutfeld and H. F. Budd, "Laser Generated MHz Elastic Waves from Metallic-Liquid Interfaces," Appl. Phys. Lett. 34, 617 (1979).

R. J. von Gutfeld, "Thermoelastic Generation of Elastic Waves for Nondestructive Testing and Medical Diagnostics," to be published, Ultrasonics, Great Britain, July 1980.

P. J. Westervelt and R. S. Larson, "Laser Excited Broadside Array," J. Acous. Soc. of America 54, 121 (1973).

R. M. White, "Generation of Elastic Waves by Transient Surface Heating," J. Appl. Phys. 34, 3559 (1963).

H. K. Wikramasinghe, R. C. Bray, V. Jipson, C. F. Quate and J. R. Salcedo, "Photoacoustics on a Microscopic Scale," Appl. Phys. Lett. 33, 923 (1978).

VII. CONCLUSIONS AND RECOMMENDATIONS

We have demonstrated a number of techniques utilizing lasers to generate MHz elastic waves for the purpose of nondestructive testing. The advantages of the laser technique lie chiefly in the ability to 1) scan the acoustic excitation source and 2) obtain very small excitation spot sizes. The addition of optical modulation of a CW light source at frequencies up to ~ 50 MHz makes it possible to generate high frequency elastic waves relatively efficiently. It is therefore possible to perform flaw detection measurements over very small regions and complicated surface geometries when, for example, the object is clamped by a layer of water.

Although we have not performed flaw detection measurements above 20 MHz, it is apparent that the techniques we have demonstrated can be extended to higher frequencies. For high data rates it is important to consider the effect of the laser pulses on the temperature rise of the absorbing region. Under those conditions it is important to optimize the conversion efficiency (from optical to elastic energy) at the desired elastic wave frequency and to minimize the temperature rise of the sample under test. It appears that mode-locked lasers offer the most attractive possibilities for high frequency elastic wave generation as already demonstrated by Brienza et al[15] and Wikramasinghe et al[16] in the 1 GHz range. Alternatively, optoacoustic modulation of CW lasers offers a potentially flexible high frequency source of laser generated elastic waves.

We have found both experimentally and theoretically that the conversion efficiency is generally an order of magnitude lower than that obtainable from piezoelectric generators. However, the other advantages discussed in this report make laser generated waves an attractive alternative and in some cases a unique choice for certain nondestructive testing applications.

FIGURE CAPTIONS

Fig. 1 Microscope stage acoustic water tank showing flaw detection of small specimen submerged with water as the clamp. Sample movement is via the micrometer screw.

Fig. 2 Same as Fig. 1 except here a rubber membrane is interposed between sample and laser to serve as the elastic wave generator.

Fig. 3 10 MHz data using 5 nsec pulses to interrogate an Al sample 0.32 cm thick. Edge holes, 2 mm deep serve as the flaw with diameters 1) 0.036 cm, 2) 0.055 cm, 3) 0.092 cm and 4) 0.1 cm. The numbers are positioned at the location of the flaws. The flaw at 5) is a crack caused by the joint between the sample and its support.

Fig. 4 Transmission data for the same sample as Fig. 3 taken with two 10 MHz piezoelectric transducers, a 6 mm diameter immersion transducer replacing the laser as the generator. Note the lack of resolution compared to Fig. 3.

Fig. 5 Transmission data for a Ti sample irradiated with the laser set-up at 10 MHz as in Fig. 1. Data is shown here for the laser absorbed directly above the through holes A–D and two regions above solid Ti, i.e. no holes. The holes have diameters, A = 0.2 cm, B = 0.14 cm, C = 0.1 cm and D = 0.05 cm.

Fig. 6 Data for laser generated elastic waves in transmission through 5μ thick copper lines on a thin base of copper-chrome on glass. The transmission data is shown for varying widths of thick and thin lines (see text). A clear distinction between thick and thin lines is obtained.

Fig. 7 Transmission data at 10 MHz through a section of graphite-epoxy, with a missing lamination, marked on the diagram as defect. Excitation is with 5 nsec laser pulses absorbed directly on the epoxy board 7a; using a rubber membrane, 7b to act as generating surface.

Fig. 8 Transmission data as above, but with two 10 MHz detectors. Considerably less detail in the data results compared to Fig. 7.

Fig. 9 The temperature-time history for a gold film evaporated onto an α-quartz substrate shown with and without a glass clamp. Two pulse widths, 1 nsec and 10 nsec are shown. The model assumes 1 dimensional heat flow, uniform heating for 1 W/cm^2 absorbed by the gold.

Fig. 10 Temperature time history for a 10 nsec pulse applied to a glass-Au-α-quartz sample. The upper cooling curve is for 1 dimensional heat flow, the lower trace for 3 dimensional heat flow. For this time scale, both the 1 dimensional and 3 dimensional cases have identical heating portions for the 5×10^{-3} cm gaussian beam radius (see text).

Fig. 11 Thermal profile for 5 nsec pulses incident at a water-steel and water-Al interface for a guassian beam with $r_o = 5 \times 10^{-3}$ cm. Note that the interface temperature stays below the water boiling of point for power densities 10^6 W/cm^2 at the center of the gaussian beam.

Fig. 12 Water tank showing moveable 10 MHz detector for measurements of transmitted elastic waves as a function of position. The laser is incident at a thin film-glass interface generating thermoelastic waves in the water.

Fig. 13 Computer graphics display of the acoustic field at 10 MHz (vertical scale) as a function of position in a water tank for a thin film heated by a pulsed Nd-YAG laser.

Fig. 14 Photoacoustic plexiglass cell with a cell volume of ~ 0.2 cm^3. Laser radiation can be applied through the cell window as shown, or to the back of the sample.

Fig. 15 Plexiglass cell containing cylindrical PZT to detect acoustic waves via an oscillating thermal pressure wave in water. The cell can also be used to detect acoustic waves transmitted from the sample to the liquid (see text).

Fig. 16 Data for stainless steel samples of varying thicknesses used in conjunction with the cell of Fig. 15. The frequency dependence agrees approximately with that predicted by Eq. 7.

VIII. REFERENCES

1. R. J. von Gutfeld and R. L. Melcher, "20 MHz Acoustic Waves from Pulsed Thermoelastic Expansion of Constrained Surfaces," Appl. Phys. Lett. 30, 257 (1979).

2. R. J. von Gutfeld and R. L. Melcher, "MHz Acoustic Waves from Pulsed Thermoelastic Expansion and Their Application to Flaw Detection," Mat. Evaluation 35, 97 (1977).

3. R. J. von Gutfeld, to be published, Ultrasonics, July 1980.

4. A. Rosencwaig and G. Busse, "High-Resolution Photoacoustic Thermal Wave Microscopy," Electron. Lett. 15, 326 (1979).

5. M. Luukkala and A. Penttinen, "Photoacoustic Microscopy," Electron. Lett. 15, 326 (1979).

6. R. J. von Gutfeld and H. F. Budd, "Laser Generated MHz Elastic Waves from Metallic-Liquid Interfaces," Appl. Phys. Lett. 34, 617 (1979).

7. L. G. Pittaway, "The Temperature Distribution in Thin Foil and Semi-infinite Targets Bombarded by an Electron Beam," British Journal of Applied Physics 15, 967 (1964).

8. M. Born and E. Wolf, "Principles of Optics," Pergamon Press, New York (1959).

9. R. M. White, "Generation of Elastic Waves by Transient Surface Heating," J. Appl. Phys. 34, 3559 (1963).

10. R. J. von Gutfeld and H. F. Budd, "Thermoelastic Generation of MHz Waves at Metallic Liquid Interfaces, Bull. of Am. Phys. Soc. 24, 253 (1979).

11. Private communication.

12. A. C. Tam and Y. H. Wong, "Optimization of Optoacoustic Cell for Depth Profiling Studies of Semiconductor Surfaces," Appl. Phys. Lett. 36, 471 (1980).

13. A. C. Tam and C. K. N. Patel, "Optical Absorptions of Light and Heavy Water by Laser Optoacoustic Spectroscopy," Applied Optics 18, 3348 (1979).

14. G. Busse and A. Rosencwaig, "Subsurface Imaging with Photoacoustics," Appl. Phys. Lett. 36, 815 (1980).

15. M. J. Brinza and A. J. DeMaria, "Laser-Induced Microwave Sound by Surface Heating," Appl. Phys. Lett. 11, 44 (1967).

16. H. K. Wikramasinghe, R. C. Bray, V. Jipson, C. F. Quate and J. R. Salcedo, "Photoacoustics on a Microscopic Scale, Appl. Phys. Lett. 33, 923 (1978).

IX ACKNOWLEDGMENTS

I am grateful to Dr. H. F. Budd for his help with the thermal profile calculations, to Drs. A. Duerinckx, S. S. Wang and C. N. Liu for the computer graphics and Dr. R. Hodgson for the use of his Nd-YAG laser. The technical assistance of Mr. D. R. Vigliotti throughout the term of the contract has been indispensable.

I would also like to acknowledge several helpful discussions with Dr. W. Scott of NADC.

D I S T R I B U T I O N L I S T

Commander Naval Air Systems Command (AIR-954) Department of the Navy Washington, DC 20361	2 COPIES
Commander Naval Air Systems Command (AIR-320) Department of the Navy Washington, DC 20361	1 COPY
Commander Naval Air Systems Command (AIR-4114C) Department of the Navy Washington, DC 20361	1 COPY
Commander Naval Air Systems Command (AIR-5203) Department of the Navy Washington, DC 20361	1 COPY
Commander Naval Air Systems Command (AIR-52031B) Department of the Navy Washington, DC 20361	1 COPY
Commander Naval Air Systems Command (AIR-52032) Department of the Navy Washington, DC 20361	1 COPY
Commander Naval Air Systems Command (AIR-52032D) Department of the Navy Washington, DC 20361	1 COPY
Dr. Robert Crane (AFML/LLP) Wright-Patterson Air Force Base Air Force Materials Laboratory Dayton, OH 45433	1 COPY
Mr. N. Tideswell (Code 2823) David W. Taylor Naval Ship R&D Center Annapolis, MD 21402	1 COPY
Mr. S. Friedman (Code 2823) David W. Taylor Naval Ship R&D Center Annapolis, MD 21402	1 COPY

D I S T R I B U T I O N L I S T

Mr. D. Polansky Naval Surface Weapons Center White Oak Silver Spring, MD 20910	1 COPY
Mr. J. R. Gleim Naval Ship Engineering Center Washington, DC 20362	1 COPY
Mr. J. F. Goff Naval Surface Weapons Center White Oak Silver Spring, MD 20910	1 COPY
Mr. J. R. Lowney Naval Surface Weapons Center White Oak Silver Spring, MD 20910	1 COPY
Mr. G. V. Blessing Naval Surface Weapons Center White Oak Silver Spring, MD 20910	1 COPY
Dr. M. I. Jacobson Lockheed Missles & Space Company, Inc. Sunnyvale, CA 94088	1 COPY
Mr. S. D. Hart(Code 8435) Naval Research Laboratory Washington, DC 20375	1 COPY
Mr. I. Wolock (Code 8433) Naval Research Laboratory Washington, DC 20375	1 COPY
Mr. C. Anderson Naval Surface Weapons Center Dahlgren, VA 22448	1 COPY
Mr. D. Nesterok (Code 92713) Naval Air Engineering Center Lakehurst, NJ 08723	1 COPY

D I S T R I B U T I O N L I S T

Mr. R. Deitrich (Code 92713) Naval Air Engineering Center Lakehurst, NJ 08723	1 COPY
Mr. J. M. Warren Naval Surface Weapons Center White Oak Silver Spring, MD 20910	1 COPY
Dr. W. J. Renton Manager - Advanced Composites Vought Corporation Post Office Box 6144 Dallas, TX 75222	1 COPY
Dr. C. Sanday (Code 6370) Naval Research Laboratory Washington, DC 20375	1 COPY
Dr. R. Weimer (Code 6370) Naval Research Laboratory Washington, DC 20375	1 COPY
Administrator Defense Documentation Center for Scientific and Technical Information (DDC) Bldg. #5, Cameron Station Alexandria, VA 22314	12 COPIES
Commander Naval Air Development Center (Code 813) Warminster, PA 18974	3 COPIES